ARTICLE

Check for updates

Warming, increase in precipitation, and irrigation enhance greening in High Mountain Asia

Fadji Zaouna Maina[1,2 ✉], Sujay V. Kumar [1], Clement Albergel[3] & Sarith P. Mahanama[1,4]

High-Mountain Asia exhibits one of the highest increases in vegetation greenness on Earth, subsequently influencing the exchange of water and energy between the land surface and the atmosphere. Given the strong interactions between the hydrosphere, the biosphere, and the cryosphere, understanding the drivers of greening in this highly complex region with significant land cover heterogeneity is essential to assess the changes in the regional water budget. Here, we perform a holistic multivariate remote sensing analysis to simultaneously examine the primary components of the terrestrial water cycle from 2003 to 2020 and decipher the principal drivers of greening in High-Mountain Asia. We identified three drivers of greening: (1) precipitation drives greening in mid and low elevation areas covered by evergreen and mixed forests (e.g., Irrawaddy basin), (2) decreases in snow enhance greening in most of the hydrologic basins, and (3) irrigation induces greening in irrigated lands (Ganges–Brahmaputra and Indus).

[1] NASA Goddard Space Flight Center, Hydrological Sciences Laboratory, Greenbelt, MD, USA. [2] Universities Space Research Association, Goddard Earth Sciences Technology and Research Studies and Investigations, Columbia, MD, USA. [3] European Space Agency Climate Office, ECSAT, Harwell Campus, Oxfordshire, Didcot OX110FD, UK. [4] Science Applications International Corporation, McLean, VA, USA. ✉email: fadjizaouna.maina@nasa.gov

Understanding changes in vegetation, a key component of the biosphere, is critical to improving our ability to predict, mitigate, and adapt to future changes in climate[1]. Over the past decades, satellites enabling large-scale vegetation monitoring such as measurements of leaf area index (LAI) have revealed that our planet is greening[2–6]. While greening is primarily caused by CO_2 fertilization[2,3,7–10], it could also potentially be attributed to or exacerbated locally by land management and precipitation trends[3]. Earth's greening impacts hydrologic connectivity and fluxes[4,7,11,12] as well as atmospheric dynamics[13,14]. Therefore, assessing greening drivers is essential to deepen our understanding of the two-way interactions between the changes in the biosphere and the hydrosphere, which in turn, is crucial to improving our understanding of the movement and transfer of water and energy from the subsurface to the atmosphere.

High Mountain Asia (HMA), a high-elevation geographical area (considered as the region from 20°N to 46°N, and 60°E to 111°E here), includes the Asian mountain ranges surrounding the Tibetan Plateau (Fig. 1) and hosts the world's largest reservoirs of glaciers, ice, and snow outside the polar regions. Multiple processes control its terrestrial water budget including cryospheric sources of water (snow, glacier, and permafrost melting), monsoon and westerlies dynamics, and anthropogenic activities such as irrigation and pumping. The region encompasses many important and large-scale hydrologic basins (e.g., the Ganges–Brahmaputra, the Indus, and the Yangtze) and is home to over a billion people, who rely on its water towers[15,16] for agriculture, ecosystems preservation, livelihood, and energy. The

topography, hydroclimate, and vegetation of HMA are highly heterogeneous. Elevation ranges from the sea level to the world's highest point (i.e., Mount Everest), and the land cover includes evergreen forest, croplands, grasslands, and bare soil.

HMA is already experiencing the impacts of global warming[17,18], which includes both changes in precipitation and increases in temperature[19–24] at an alarming rate. In addition, India and China have one of the highest rates of greening on Earth[19,25–29] that could be attributed to changes in climate[24,30,31], land use, and land cover[2,25,27]. While ~79% of greening on Earth is attributed to CO_2 fertilization and nitrogen deposition[2,3], in HMA, the high increases in vegetation greenness are moisture induced[32] and are caused by changes in climate and land use[2,3]. In this study, we analyze how climatic and anthropogenic factors affect the moisture induced greening in HMA. A better understanding of the drivers of greening in HMA will provide insights into its impacts on water resources as well as the interactions between the land and the atmosphere[21,29,33,34]. Here we employ a holistic approach that simultaneously analyzes multiple processes at the interface of water and vegetation dynamics to identify the principal drivers of greening. We utilize a large set of remote sensing products to study the water and energy cycle changes from 2003 to 2020. The increase in vegetation greenness is quantified using the LAI data provided by MCD15A2H Version 6 Moderate Resolution Imaging Spectroradiometer (MODIS)[35]. We then link these changes to the above and below root zone hydrodynamics as well as atmospheric processes. Specifically, the key land surface processes (snow dynamics by analyzing the snow
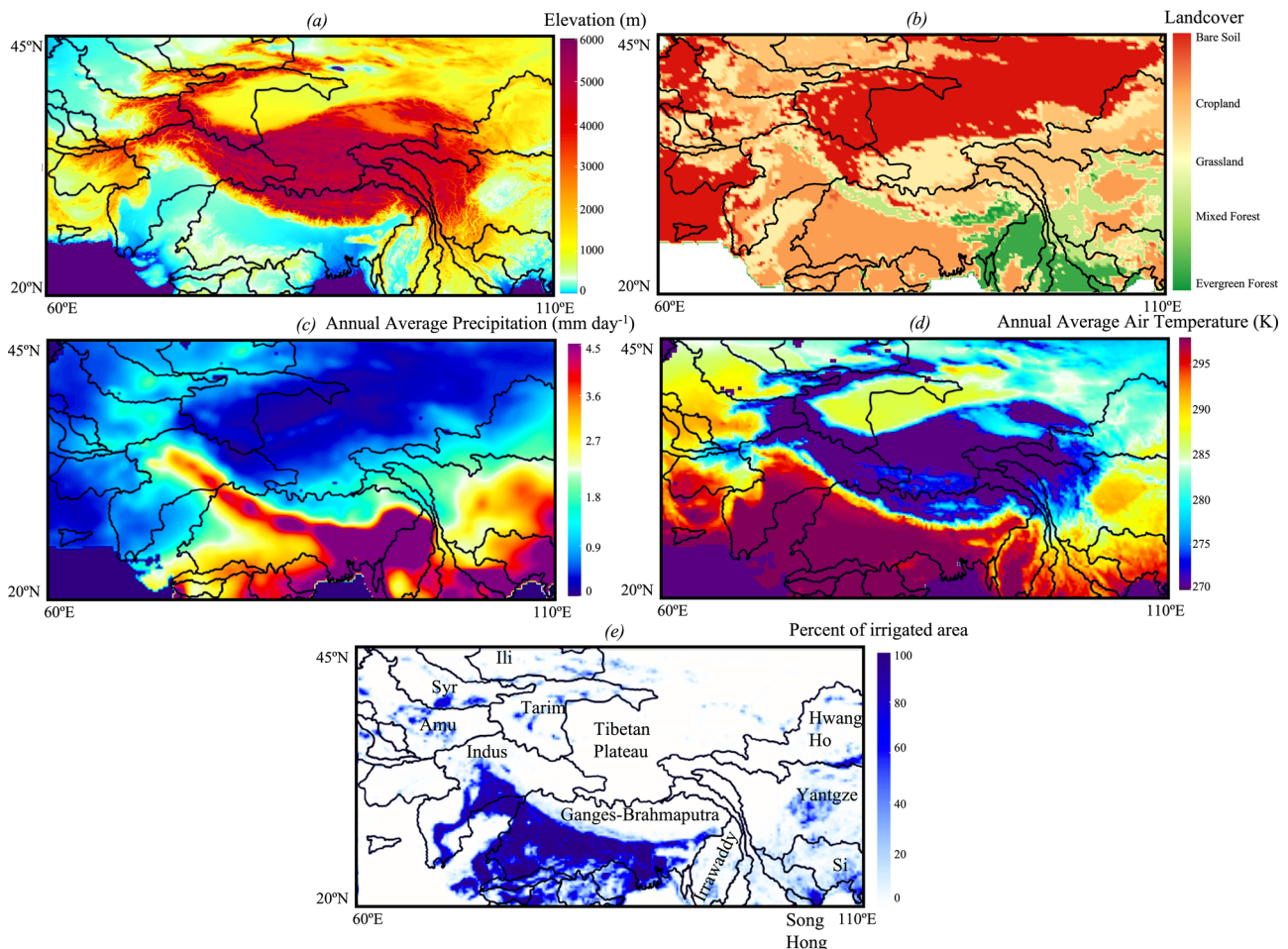

Fig. 1 Maps of High Mountain Asia. a elevation, b land cover[99], c average annual IMERG precipitation and d air temperature from 2003 to 2020 from ERA5, and e percent of irrigated areas per pixel[41]. The black lines indicate the limits of the hydrologic basins and their names are indicated in (e).

cover fraction provided by MODIS MOD10CM[36] and soil moisture provided by the European Space Agency Climate Change Initiative ESA CCI[37]) and the variations of the terrestrial water storages measured by the Gravity Recovery And Climate Experiment GRACE[38] are examined here. These changes in water availability enabling greening are then linked to either anthropogenic activities (i.e., irrigation) or changes in atmospheric conditions (i.e., precipitation and air temperature) by analyzing gridded surface meteorology products, including ECMWF's fifth generation of atmospheric reanalysis of the global climate ERA5[39] and the Final product of the Integrated Multi-satellitE Retrievals for Global Precipitation Measurement IMERG[40]. Our study shows that depending on the elevation, the land cover, and the land use, greening in HMA is driven by three main factors: intense irrigation, decreases in snow cover, and an increase in precipitation. The spatial distribution of the relative influence of these factors is captured in Fig. 2.

Results

The increase in vegetation greenness is highly heterogenous in HMA. Regions located in low and mid-elevation (<4000 m) have the highest rates of increase (Supplementary Fig. 1). Changes in LAI also depend on the type of land cover: evergreen and mixed forests representing around 13% of HMA have an increase in LAI equal to 0.011 $m^2m^{-2}year^{-1}$, croplands covering ~18% of HMA have an increasing trend of LAI equal to 0.01 $m^2m^{-2}year^{-1}$, and grasslands covering ~16% of HMA have an increasing trend of LAI equal to 0.0036 $m^2m^{-2}year^{-1}$ on average.

Irrigation-induced greening. Increases in vegetation greenness stemming from agricultural practices mainly appear in the Ganges–Brahmaputra and the Indus basins, the two agricultural and densely populated hydrologic basins in HMA where intense irrigation[41] and pumping[42] occur. Moreover, croplands of these two basins show the highest increases in LAI in HMA (up to 0.04 $m^2m^{-2}year^{-1}$ in the Ganges–Brahmaputra and 0.03 $m^2m^{-2}year^{-1}$ in the Indus), these results are similar to the ones documented in the previous works[3,43]. Besides, the world's highest TWS decreases are found in this area (up to −10 cm/year in the Ganges–Brahmaputra and 4 cm year^{-1} in the Indus, Supplementary Figs. 2 and 3), similar to the previous works[42,44–46]. Groundwater provides approximately 60% of the water used for irrigation and over 80% of the rural and urban domestic water supplies in India originate from groundwater, making India the world's largest user of groundwater[47]. Groundwater withdrawals deplete the aquifers and yield a decrease in TWS whereas irrigation adds more water in the soil, increasing the soil moisture. Figure 3 shows the unique contributions of soil moisture and snow cover to
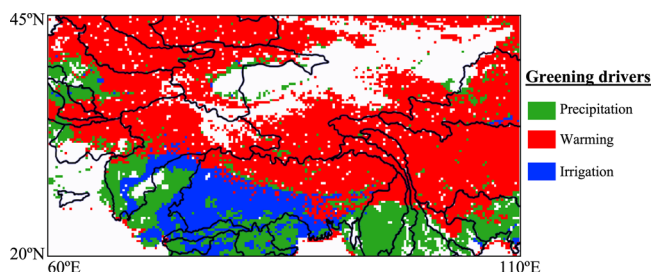

Fig. 2 Spatial distribution of the principal drivers of greening in HMA. Precipitation-driven greening is observed in areas where the information about LAI from precipitation/soil moisture is the highest. Warming-induced greening is limited to areas where the information from snow cover about LAI is the highest. Irrigation-induced greening is observed in irrigated lands where the information about LAI from soil moisture is the highest.
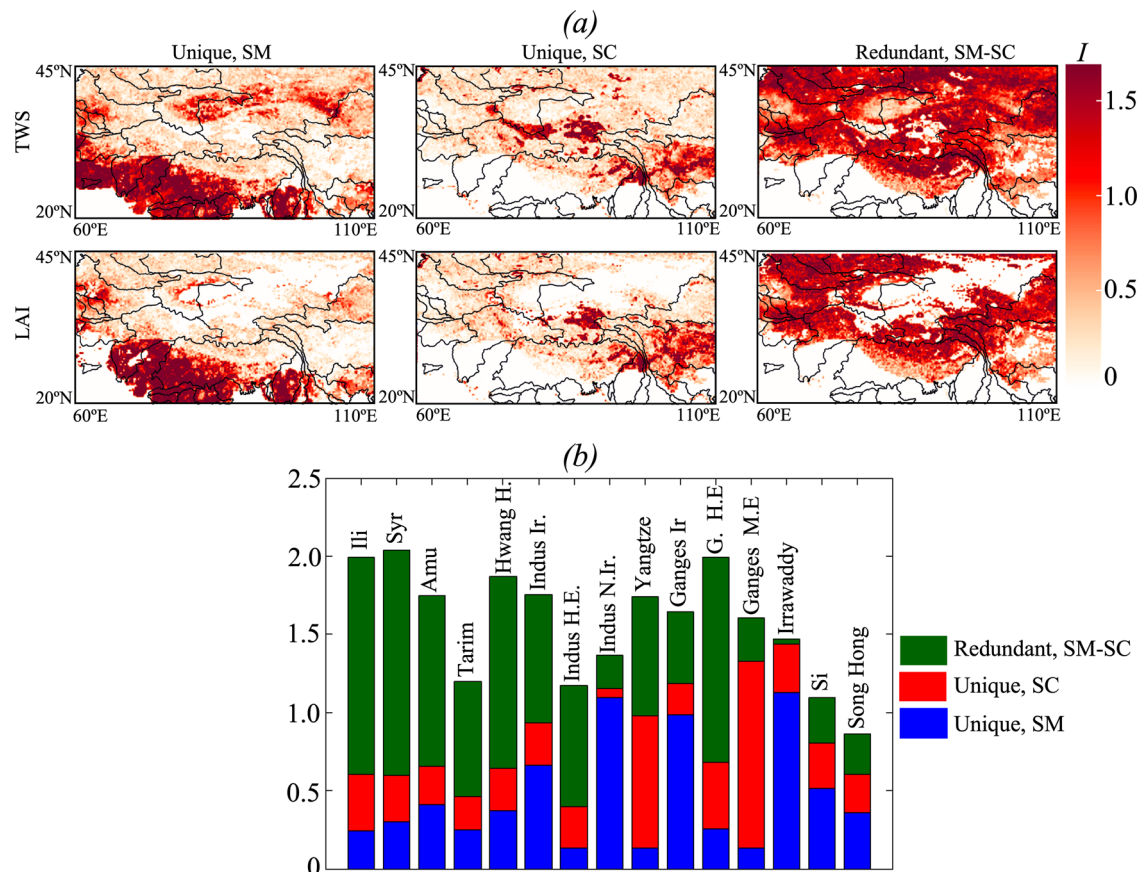
TWS and LAI changes using a non-parameteric information theory analysis (Section 4.2). As shown in Fig. 3a, the partial information decomposition of TWS is strongly linked to the changes in soil moisture, over Indus and Ganges–Brahmaputra. Increases in soil moisture by irrigation led to more water available to sustain the crops and to enhance vegetation greenness[25,32,43,48]. Consequently, increases in LAI are mainly driven by the changes in soil moisture, as indicated by the unique information of soil moisture (Fig. 3a, b). The low unique and redundant information of precipitation and temperature about the soil moisture in the area (Fig. 4) confirms that the increases in soil moisture at a rate equal to ~2%/year (Supplementary Figs. 2 and 3) are neither linked to precipitation nor temperature rather the intense water applied through irrigation despite an increasing trend of precipitation equal to 0.06 mm day^{-1}year^{-1} (Supplementary Figs. 2 and 3) in some gridded products.

Warming-induced greening. Here, we refer to warming-induced greening as a consequence of the increase in soil moisture deriving from the decreases in snow rather than the direct impact from increase in air temperature. The increase in air temperature in HMA (up to 0.6 °C on average in the Tibetan Plateau and other areas subject to strong interactions with the cryosphere such as the mountain ranges of the Hindu Kush and Pamir) has led to a decrease in snow cover fraction (>−0.4% year^{-1}) and an increase in soil moisture (up to 1% year^{-1}; Supplementary Fig. 2). As a result, there is more water available for vegetation growth[49–51]. Moreover, warming tends to shorten the snow accumulation time[52], which increases the growing season for vegetation. In these basins, changes in LAI and TWS are due to both the variations of snow cover fraction and soil moisture due to their interdependence (Fig. 3a, b). We attribute greening to the decreases in snow cover as it causes the soil moisture to increase. As such, the direct impact of temperature on soil moisture is low. Greening in response to the decreases in snow is observed in eight out of eleven HMA hydrologic basins. While only a small portion of greening in the Ganges–Brahmaputra and the Indus is controlled by the decreases in snow cover fraction, increases in vegetation greenness in the Tibetan Plateau, Hwang Ho, Ili, Amu Darya, Syr Darya, and Tarim are mostly driven by warming.

TWS at the boundary of the Tibetan Plateau is uniquely controlled by the changes in snow cover whereas both soil moisture and snow cover contribute to the changes in TWS in the center portion of the Tibetan Plateau (Fig. 3a). The Tibetan Plateau, experiencing one of the highest rates of warming in the world[17,53–57] depicts a decrease in the annual snow cover fraction (Supplementary Fig. 2), however, only summer and fall snow cover sees a significant decrease while snow cover fraction in winter tends to increase[58,59]. This is due to an increase in precipitation at a rate varying from between 0.01 to 0.04 mm day^{-1}year^{-1} (Supplementary Fig. 2) on average depending on the dataset. The observed warming in the Tibetan Plateau is likely not sufficient to shift the precipitation phase. Because both precipitation and temperature move to a direction favorable to greening, the small increases in LAI in the Tibetan Plateau are driven by both soil moisture and snow cover fraction (Fig. 3a and b), which create more water available for vegetation growth and longer growing seasons. As in this work, previous studies have attributed greening in the Tibetan Plateau to both changes in temperature and precipitation; besides, some studies have shown that the increases in temperature lead to conditions amenable to the plant activity in addition to enhancing photosynthesis and leading to a longer growing season[24,60,61].

Despite an increase in precipitation in the Yangtze (with an average rate equal to 0.03 mm day^{-1}year^{-1}; Supplementary

Fig. 3 Contributions of soil moisture and snow cover to the changes in Terrestrial Water Storage (TWS) and Leaf Area Index (LAI). a Spatial distributions of the unique and redundant information of soil moisture (SM) and snow cover (SC) in the Terrestrial Water Storage (TWS) and Leaf Area Index (LAI). **b** Average basins and sub-basins values of the unique and redundant information of soil moisture (SM) and snow cover (SC) in the Leaf Area Index (LAI). Ir is irrigated lands, N.Ir. non irrigated lands, H.E high elevation, and M.E mid-elevation. Because the synergistic information has very low values, we only show the unique and redundant information.
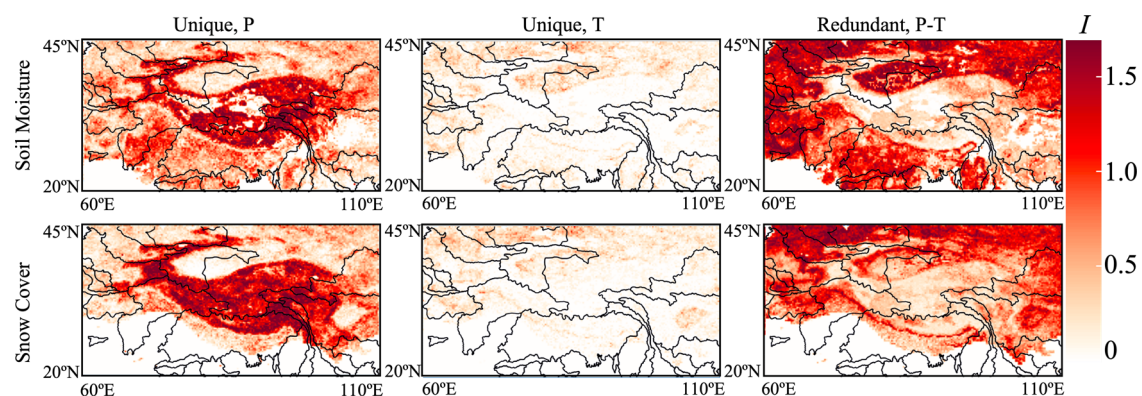

Fig. 4 Contributions of precipitation and temperature to the changes in soil moisture and snow cover. Spatial distributions of the unique and redundant information of precipitation (P) and temperature (T) in the soil moisture (SM) and snow cover (SC). Because the synergistic information has very low values, we only show the unique and redundant information.

information, Fig. 1) resulting from an increase in frequency and intensity of extreme precipitation[62,63], snow cover decreases due to increased air temperature (~0.2 °C year^{-1}). Greening in this portion of the Yangtze basin where the elevation is higher than 1500 m is predominantly controlled by the decreases in snow cover as the unique information of soil moisture about LAI as well as the redundant information between soil moisture and snow cover are low (Fig. 3a and b). This is because summer and fall snow cover in this area covered by mixed forest has decreased,

which led to a longer growing season and subsequently an increase in vegetation greenness.

In the Ganges–Brahmaputra and the Indus, the decrease in TWS in response to the decrease in the cryospheric storages is restricted to certain elevation ranges (elevation > 3000 m) and landcover type (a mixture of evergreen and mixed forests). However, the magnitude of the TWS trends (~0.1 cm year^{-1}) is lower than in the irrigated lands. Both soil moisture and snow cover control TWS and LAI as indicated by the partial

information decomposition (Fig. 3a and b). The decreases in snow cover fraction and the resulting increases in soil moisture cause the LAI to increase at a rate equal to 0.02 m^{2}m^{-2}year^{-1}.

The Hwang Ho basin is a high-elevation (elevation greater than 1000 m) basin located in the eastern part of HMA characterized by a decreasing snow cover fraction (Supplementary Fig. 5). Although the precipitation increases, TWS decreases (~1 cm year^{-1}), a consequence of an increase in air temperature (~0.1 °C year^{-1}). The high redundant information of soil moisture and snow cover about LAI indicates that the decrease in snow leads to an increase in soil moisture which in turn enhances vegetation growth (Fig. 3 a and b). A similar phenomenon is observed in the Northwestern basins (Ili, Syr Darya, Amu Darya, and Tarim). However, in these basins, the yearly changes in LAI are low (inferior to 0.01 m^{2}m^{-2}year^{-1}) even though the decreases in snow cover fraction (superior to −0.4% year^{-1}) are the highest. These changes in cryospheric storages sustaining the growth of vegetation lead, however, to a decrease in TWS (up to 1 cm year^{-1}) despite the increase of the westerlies precipitation (~0.05–0.07 mm day^{-1}year^{-1}, Supplementary Figs. 2 and 5).

Precipitation-driven greening. Precipitation-driven greening is observed in mid and low elevation areas covered by evergreen and mixed forests located in the southeast of HMA encompassing some portions of the non irrigated lands of the Indus and the monsoon-dominated climate basins (Irrawaddy, Si, and Song Hong)[64,65]. In these areas, soil moisture unique information about TWS and LAI is the highest and snow plays a smaller role (Fig. 3a, b). The partial information decomposition also shows that changes in soil moisture are mostly a result of the variations of precipitation (Fig. 4). All studied precipitation products show an increasing trend of precipitation in the non irrigated lands of the Indus (0.03 mm day^{-1}year^{-1} to 0.08 mm day^{-1}year^{-1} depending on the product, Supplementary Fig. 1) which translates into an increase in TWS (<0.1 cm year^{-1}). Likewise, precipitation in the monsoon-dominated climate basins has seen an increase (~1 mm day^{-1}year^{-1}), however, the TWS has a small decrease that could be attributed to the decreases in TWS in some years because of anthropogenic activities. In the Si and Song Hong basins, TWS decreases significantly from 2003 to 2006 (Supplementary Fig. 4) likely due to a substantial increase in groundwater abstraction for agriculture and public water supplies[64,66] in addition to the drought that the region experienced during that period[67]. In the Irrawaddy basin, a sustained decrease in TWS is observed, more prominently from 2012 to 2020 (Supplementary Fig. 4). As both precipitation and soil moisture are increasing during that period, the decreases in TWS are likely related to surface water diversion or pumping. Yearly changes in precipitation and LAI although nonmonotonic, are similar. For example, LAI decreases from 2003 to 2011 then increases, a similar pattern is observed with precipitation, soil moisture, and TWS (Supplementary Fig. 4). This reinforces the fact that vegetation changes in these regions are mainly driven by the changes in precipitation.

Discussion
Irrigation-induced greening affects more than 50% of the Ganges–Brahmaputra basin and around 22% of the Indus basin and leads to the highest increases in LAI in HMA. By altering the vegetation dynamics, changes in soil moisture induced by intense irrigation could strongly affect the interactions between the land surface and the atmosphere[68] and ultimately the climate dynamics. A slight decrease (<0.03 °C year^{-1}) in air temperature in the irrigation and precipitation-controlled greening area (Ganges–Brahmaputra, Indus, and Irrawaddy) is observed

contrary to the warming-induced greening zone, likely due to the cooling effects of an increasing vegetation[1]. Warming-induced greening areas experience an increase in precipitation likely due to the increase in temperature[17,69–72], which will further enhance greening.

Increasing trends of LAI in China (i.e., the Yangtze basin) have been attributed to afforestation[25,27]. Afforestation programs certainly may be contributing to the greening in the region, yet our study highlights that the main driver of greening in the area is the climate, and greening is observed in all the four major hydrologic basins characterized by forests (evergreen and mixed) that comprise the area though these basins are in different countries. While increases in precipitation can induce vegetation growth, an increase in vegetation greenness could also lead to an increase in precipitation by altering the interactions between the land surface and the atmosphere. However, the temporal scale at which vegetation growth from afforestation impacts the Earth system and the atmospheric dynamics to contribute to an increasing pattern of precipitation is much longer than the scale at which increasing precipitation impacts the growth of forests.

Assessing the principal drivers of greening is essential to better understand the interactions between the hydrosphere, the cryosphere, and the biosphere especially in HMA where these interactions are strong and steadily govern the water and energy cycles. With the onset of global warming, greening may lead to both cooling by increasing the evapotranspiration and warming by decreasing the albedo. This study shows that in the most two populated and heavily irrigated hydrologic basins of HMA (Ganges–Brahmaputra and Indus), greening is triggered by human activities. Proper accounting of these practices to accurately represent their dynamics and impacts is important in Earth system models and future projections of the changes in water, energy, and biogeochemical cycles.

Methods
Selected remote sensing products. We perform a multivariate analysis of remote sensing products to quantify the changes in vegetation and their links to the changes in either soil moisture or snow cover. We then study how irrigation and meteorological conditions (temperature and precipitation) affect the variations of soil moisture and snow cover.

MODIS LAI. Changes in LAI are good indicators of greening or browning in a given area and have been previously used to analyze changes in vegetation on Earth[2,3,6,73]. LAI, defined as the total area of leaves over a unit of ground area, characterizes the plant canopy and determines the size of the interface for the exchange of energy and mass between the canopy and the atmosphere. We study the LAI values provided by the MCD15A2H Version 6 of MODIS[35] at a spatial resolution of 500 m and a temporal resolution equal to 8 days.

Gridded surface meteorology datasets. Vegetation dynamics strongly depend on the atmospheric conditions, notably precipitation and air temperature. Because precipitation, is highly uncertain in HMA[74,75] due to the lack of adequate ground-based measurements resulting from the difficulty of access, the harsh environments, and the geographical complexities of the region[76], we analyze widely used gridded datasets derived from reanalysis and/or satellite-based products[76–80]: ERA5, IMERG, CHIRPS, APHRODITE, HAR, and PRINCETON. The fifth generation ECMWF atmospheric reanalysis of the global climate ERA5 provides hourly estimates of precipitation by combining satellite and in-situ data into global estimates using advanced modeling and data assimilation systems on a 30 km grid[39]. GPM IMERG uses information from the GPM satellite constellation to estimate precipitation over the Earth's surface at a spatial resolution of 10 km[40]. CHIRPS, a thermal infrared-based dataset, incorporates both the Tropical Rainfall Measuring Mission Multi-satellite Precipitation Analysis and gauge products and provides a quasi-global precipitation dataset at a resolution of 0.05°[81]. APHRO-DITE product is a daily gridded precipitation dataset for Asia that is generated from a dense network of daily rain-gauge data[82]. HAR is an atmospheric dataset generated primarily for the Tibetan Plateau by dynamical downscaling of the final operational global analysis using the Weather Research and Forecasting regional mesoscale model[83]. The global meteorological dataset for land surface modeling provided by PRINCETON[84] derived from a reanalysis of land surface models and other terrestrial modeling systems (e.g., the global precipitation climatology project daily precipitation, the tropical rainfall measuring mission, and NASA Langley

monthly surface radiation budget) provides precipitation at a spatial resolution of 1°. We use ERA5 air temperature to assess the changes in air temperature in the region over the past two decades.

MODIS snow cover fraction. Snow is a critical component of the hydrological system and drives the vegetation ecosystem in high altitude mountainous regions. To evaluate the impacts of the changes in snow on vegetation greenness, we use the monthly snow cover fraction estimates provided by MODIS Snow Cover fraction L3 MOD10CM at a spatial resolution of 0.05°[36].

ESA CCI soil moisture. Soil moisture plays a significant role in vegetation growth and dynamics. To understand the changes in vegetation greenness, we analyze the daily soil moisture provided by the ESA CCI v05.2. We use the combined dataset generated by blending the soil moisture retrievals from active and passive micro-wave remote sensing instruments.

GRACE TWS. TWS includes all types of water stored above and below the ground surface such as snow, ice, groundwater, and surface water storage. Changes in TWS can also be used as a measure of the interactions between the changes in water storage and vegetation. We quantify changes in TWS by analyzing GRACE[38,85] CSR RL06 mass concentrations (mascons)[86] datasets. GRACE provides changes in TWS on a global scale at a resolution of 300–500 km[85,87,88]. Although previous studies have advised using GRACE only over large-scale basins with areas greater than 250,000 km^2, several studies have employed GRACE, often the only data available to study changes in water storages in HMA, to investigate the dynamics of the water cycle in this region[89–91].

Statistical analyses. We performed statistical analyses at a yearly temporal resolution and at both basin scale and the resolution of GRACE CSR RL06 mascons (i.e., 0.5°), the coarsest resolution of all remote sensing products utilized in this study. All the other remote sensing products were then upscaled to 0.5°. We computed the yearly trends of the LAI, precipitation, temperature, soil moisture, snow cover, and TWS using the Mann–Kendall test, which determines whether a time series has a monotonic upward or downward trend[92–96]. The Mann–Kendall test uses the following statistics:

$$S = \sum_{i=1}^{n-1} \sum_{j=k+1}^{n} sign(x_j - x_i) \qquad (1)$$

where x is the time series variable. The subscript j and k are the observation time. $sign(x_j - x_i)$ is equal to +1, 0, or −1, which means increasing, no, and decreasing trends, respectively. In this study, we assumed that there is no significant trend in the data at 95% confidence level (or at a significant level of 5%).

The analysis of these trends will allow us to quantify the changes of these critical land surface variables over the past decades. However, a deeper analysis of the factors controlling changes in LAI also requires the examination of the dependence between the different variables. We use the Partial Information Decomposition (PID) to quantify these interactions and dependencies. The PID, an extension of the Shannon information measures to a multivariate system, allows the calculation of (1) the amount of information that each control variable uniquely contributes to the output, (2) the redundant information (that is repeated) between the control variables, and (3) the synergistic information between the variables. Considering two random variables X_1 and X_2 sources of information of a random variable Y. The total mutual information $I(X;Y)$ between the vector of source variables X and the target variable Y is given by

$$I(X;Y) = U(X_1;Y) + U(X_2;Y) + R(X;Y) + S(X;Y) \qquad (2)$$

Where U, R, and S are the unique, redundant, and synergistic information, respectively.

The redundant information, defined as the sum of the minimum value of specific information I_{spec} provided by each source, is given by

$$R(X;Y) = \sum_{y \in Y} p(Y=y) \min\{I_{spec}(X_1;Y=y), I_{spec}(X_2;Y=y)\} \qquad (3)$$

With p being the probability distribution

The specific information quantifying the information associated with a particular outcome y of Y is

$$I_{spec}(X_1;Y=y) = \sum_x p(x|y) \left[\log \frac{1}{p(x)} - \log \frac{1}{p(y|x)} \right] \qquad (4)$$

The unique information is then equal to:

$$U(X_1;Y) = I(X_1;Y) - R(X;Y) \qquad (5)$$

$I(X_1;Y)$ is the mutual information between X_1 and Y

Then the synergistic information $S(X;Y)$ is derived from:

$$S(X;Y) = I(X;Y) - U(X_1;Y) - U(X_2;Y) - R(X;Y) \qquad (6)$$

More details about the computation of these metrics can be found in[97,98].

Because we study the dependence and the relationship between the different variables at a yearly time scale, the potential lag correlation that could exist

between precipitation, LAI, soil moisture, and snow cover is less important and is ignored here. Moreover, we only show the unique and redundant information because the synergistic information was non-significant. We first investigate the contributions of soil moisture and snow cover to the terrestrial water storages and the changes in vegetation greenness (i.e., LAI). We then analyze the factors (meteorological conditions or irrigation) governing the changes in soil moisture and snow cover. When soil moisture is predominantly driving the changes in LAI (i.e., soil moisture unique information about LAI is the highest) and the changes in soil moisture are related to changes in precipitation (i.e., precipitation unique information about soil moisture is the highest), we attribute greening to the variations of precipitation, otherwise i.e., when the increases in soil moisture are not related to the precipitation and the area is irrigated, we conclude that the observed greening stemmed from irrigation. If the snow cover unique information about LAI is the highest, greening is assumed to be driven by warming or decreases in snow cover. Because decreases in snow cover generally cause vegetation growth by increasing the soil moisture, we also assume that greening is governed by the decreases in snow cover when the redundant information between soil moisture and snow cover about LAI is the highest and the area is covered by snow.

Data availability

References

1. Zeng, Z. et al. Climate mitigation from vegetation biophysical feedbacks during the past three decades. *Nat. Clim. Change* **7**, 432–436 (2017).
2. Piao, S. et al. Characteristics, drivers and feedbacks of global greening. *Nat. Rev. Earth Environ* **1**, 14–27 (2020).
3. Zhu, Z. et al. Greening of the Earth and its drivers. *Nat. Clim. Change* **6**, 791–795 (2016).
4. Zeng, Z. et al. Impact of Earth Greening on the Terrestrial Water Cycle. *J. Clim.* **31**, 2633–2650 (2018).
5. Zhang, Y., Song, C., Band, L. E., Sun, G. & Li, J. Reanalysis of global terrestrial vegetation trends from MODIS products: Browning or greening? *Remote Sens. Environ.* **191**, 145–155 (2017).
6. Munier, S. et al. Satellite leaf area index: global scale analysis of the tendencies per vegetation type over the last 17 years. *Remote Sens* **10**, 424 (2018).
7. Los, S. O. Analysis of trends in fused AVHRR and MODIS NDVI data for 1982–2006: Indication for a CO2 fertilization effect in global vegetation. *Glob. Biogeochem. Cycles* **27**, 318–330 (2013).
8. Ukkola, A. M. et al. Reduced streamflow in water-stressed climates consistent with CO 2 effects on vegetation. *Nat. Clim. Change* **6**, 75–78 (2016).
9. Piao, S. et al. Changes in climate and land use have a larger direct impact than rising CO2 on global river runoff trends. *Proc. Natl. Acad. Sci. U. S. A.* **104**, 15242–15247 (2007).
10. Donohue, R. J., Roderick, M. L., McVicar, T. R. & Farquhar, G. D. Impact of CO2 fertilization on maximum foliage cover across the globe's warm, arid environments. *Geophys. Res. Lett.* **40**, 3031–3035 (2013).
11. Zeng, Z., Peng, L. & Piao, S. Response of terrestrial evapotranspiration to Earth's greening. *Curr. Opin. Environ. Sustain* **33**, 9–25 (2018).
12. Good, S. P., Noone, D. & Bowen, G. Hydrologic connectivity constrains partitioning of global terrestrial water fluxes. *Science* **349**, 175–177 (2015).
13. Shen, M. et al. Evaporative cooling over the Tibetan Plateau induced by vegetation growth. *Proc. Natl. Acad. Sci.* **112**, 9299–9304 (2015).
14. Forzieri, G., Alkama, R., Miralles, D. G. & Cescatti, A. Satellites reveal contrasting responses of regional climate to the widespread greening of Earth. *Science* **356**, 1180–1184 (2017).
15. Viviroli, D., Dürr, H. H., Messerli, B., Meybeck, M. & Weingartner, R. Mountains of the world, water towers for humanity: Typology, mapping, and global significance. *Water Resour. Res.* **43**, W07447 (2007).
16. Pritchard, H. D. Asia's shrinking glaciers protect large populations from drought stress. *Nature* **569**, 649–654 (2019).

17. Immerzeel, W. W., Beek, L. P. Hvan & Bierkens, M. F. P. Climate change will affect the Asian water towers. *Science* **328**, 1382–1385 (2010).
18. Yang, K. et al. Recent climate changes over the Tibetan Plateau and their impacts on energy and water cycle: A review. *Glob. Planet. Change* **112**, 79–91 (2014).
19. Xu, G. et al. Changes in vegetation growth dynamics and relations with climate over China's landmass from 1982 to 2011. *Remote Sens.* **6**, 3263–3283 (2014).
20. Yin, G., Hu, Z., Chen, X. & Tiyip, T. Vegetation dynamics and its response to climate change in Central Asia. *J. Arid Land* **8**, 375–388 (2016).
21. Gessner, U. et al. The relationship between precipitation anomalies and satellite-derived vegetation activity in Central Asia. *Glob. Planet. Change* **110**, 74–87 (2013).
22. Gao, J. et al. Past and future effects of climate change on spatially heterogeneous vegetation activity in China. *Earths Future* **5**, 679–692 (2017).
23. Li, Z., Chen, Y., Li, W., Deng, H. & Fang, G. Potential impacts of climate change on vegetation dynamics in Central Asia. *J. Geophys. Res. Atmospheres* **120**, 12345–12356 (2015).
24. Sun, J., Qin, X. & Yang, J. The response of vegetation dynamics of the different alpine grassland types to temperature and precipitation on the Tibetan Plateau. *Environ. Monit. Assess.* **188**, 20 (2016).
25. Chen, C. et al. China and India lead in greening of the world through land-use management. *Nat. Sustain* **2**, 122–129 (2019).
26. Song, X.-P. et al. Global land change from 1982 to 2016. *Nature* **560**, 639–643 (2018).
27. Zhang, Y. et al. Multiple afforestation programs accelerate the greenness in the 'Three North' region of China from 1982 to 2013. *Ecol. Indic.* **61**, 404–412 (2016).
28. Cui, X. & Graf, H.-F. Recent land cover changes on the Tibetan Plateau: a review. *Clim. Change* **94**, 47–61 (2009).
29. Zhong, L., Ma, Y., Salama, Mhd., S. & Su, Z. Assessment of vegetation dynamics and their response to variations in precipitation and temperature in the Tibetan Plateau. *Clim. Change* **103**, 519–535 (2010).
30. Ding, M. et al. The relationship between NDVI and precipitation on the Tibetan Plateau. *J. Geogr. Sci.* **17**, 259–268 (2007).
31. Wang, C. et al. Assessing phenological change and climatic control of alpine grasslands in the Tibetan Plateau with MODIS time series. *Int. J. Biometeorol.* **59**, 11–23 (2015).
32. Wang, X. et al. Moisture-induced greening of the South Asia over the past three decades. *Glob. Change Biol.* **23**, 4995–5005 (2017).
33. Huang, K. et al. The influences of climate change and human activities on vegetation dynamics in the Qinghai-Tibet Plateau. *Remote Sens* **8**, 876 (2016).
34. Peng, J., Liu, Z., Liu, Y., Wu, J. & Han, Y. Trend analysis of vegetation dynamics in Qinghai–Tibet Plateau using Hurst Exponent. *Ecol. Indic.* **14**, 28–39 (2012).
35. Myneni, R., Knyazikhin, Y. & Park, T. MOD15A2H MODIS/Terra Leaf Area Index/FPAR 8-Day L4 Global 500m SIN Grid V006. https://doi.org/10.5067/MODIS/MOD15A2H.006 (2015).
36. Hall, D. K., G. A., Riggs & Salomonson, V. V. MODIS/Terra Snow Cover 5-Min L2 Swath 500m, Version 5. https://doi.org/10.5067/ACYTYZB9BEOS (2006).
37. Dorigo, W. et al. ESA CCI soil moisture for improved Earth system understanding: state-of-the art and future directions. *Remote Sens. Environ.* **203**, 185–215 (2017).
38. Tapley, B. D., Bettadpur, S., Watkins, M. & Reigber, C. The gravity recovery and climate experiment: Mission overview and early results. *Geophys. Res. Lett.* **31**, L09607 (2004).
39. Hersbach, H. et al. The ERA5 global reanalysis. *Q. J. R. Meteorol. Soc.* **146**, 1999–2049 (2020).
40. Huffman, G. J., Bolvin, D. T. & Nelkin, E. J. Integrated multi-satellitE retrievals for GPM (IMERG) technical documentation. *NASAGSFC Code* **612**, 47 (2015).
41. Salmon, J. M., Friedl, M. A., Frolking, S., Wisser, D. & Douglas, E. M. Global rain-fed, irrigated, and paddy croplands: A new high resolution map derived from remote sensing, crop inventories and climate data. *Int. J. Appl. Earth Obs. Geoinformation* **38**, 321–334 (2015).
42. Rodell, M., Velicogna, I. & Famiglietti, J. S. Satellite-based estimates of groundwater depletion in India. *Nature* **460**, 999–1002 (2009).
43. Parida, B. R., Pandey, A. C. & Patel, N. R. Greening and browning trends of vegetation in india and their responses to climatic and non-climatic drivers. *Climate* **8**, 92 (2020).
44. Famiglietti, J. S. The global groundwater crisis. *Nat. Clim. Change* **4**, 945–948 (2014).
45. Taylor, R. G. et al. Ground water and climate change. *Nat. Clim. Change* **3**, 322–329 (2013).
46. Wada, Y. et al. Global depletion of groundwater resources. *Geophys. Res. Lett.* **37** (2010).
47. Water Home. https://www.worldbank.org/en/topic/water.

48. Sarmah, S., Jia, G. & Zhang, A. Satellite view of seasonal greenness trends and controls in South Asia. *Environ. Res. Lett.* **13**, 034026 (2018).
49. Schickhoff, U. et al. Climate change and treeline dynamics in the himalaya. in climate change, glacier response, and vegetation dynamics in the Himalaya: contributions toward future earth initiatives (eds Singh, R., Schickhoff, U. & Mal, S.) 271–306 (Springer International Publishing, 2016). https://doi.org/10.1007/978-3-319-28977-9_15.
50. Gaire, N. P., Koirala, M., Bhuju, D. R. & Borgaonkar, H. P. Treeline dynamics with climate change at the central Nepal Himalaya. *Clim. Past* **10**, 1277–1290 (2014).
51. Mainali, K. et al. Contrasting responses to climate change at Himalayan treelines revealed by population demographics of two dominant species. *Ecol. Evol.* **10**, 1209–1222 (2020).
52. Wang, X., Wu, C., Wang, H., Gonsamo, A. & Liu, Z. No evidence of widespread decline of snow cover on the Tibetan Plateau over 2000–2015. *Sci. Rep.* **7**, 14645 (2017).
53. Gao, Y. et al. Does elevation-dependent warming hold true above 5000 m elevation? Lessons from the Tibetan Plateau. *Npj Clim. Atmospheric Sci* **1**, 1–7 (2018).
54. Song, Y. et al. Agricultural adaptation to global warming in the Tibetan Plateau. *Int. J. Environ. Res. Public. Health* **16**, 3686 (2019).
55. Kang, S. et al. Review of climate and cryospheric change in the Tibetan Plateau. *Environ. Res. Lett.* **5**, 015101 (2010).
56. Duan, A. & Xiao, Z. Does the climate warming hiatus exist over the Tibetan Plateau? *Sci. Rep.* **5**, 13711 (2015).
57. Yao, T. et al. Recent third pole's rapid warming accompanies cryospheric melt and water cycle intensification and interactions between monsoon and environment: multidisciplinary approach with observations, modeling, and analysis. *Bull. Am. Meteorol. Soc* **100**, 423–444 (2019).
58. Deng, H., Pepin, N. C. & Chen, Y. Changes of snowfall under warming in the Tibetan Plateau. *J. Geophys. Res. Atmospheres* **122**, 7323–7341 (2017).
59. Tang, Z., Wang, J., Li, H. & Yan, L. Spatiotemporal changes of snow cover over the Tibetan plateau based on cloud-removed moderate resolution imaging spectroradiometer fractional snow cover product from 2001 to 2011. *J. Appl. Remote Sens.* **7**, 073582 (2013).
60. Li, B., Zhang, L., Yan, Q. & Xue, Y. Application of piecewise linear regression in the detection of vegetation greenness trends on the Tibetan Plateau. *Int. J. Remote Sens.* **35**, 1526–1539 (2014).
61. Zhang, G., Zhang, Y., Dong, J. & Xiao, X. Green-up dates in the Tibetan Plateau have continuously advanced from 1982 to 2011. *Proc. Natl. Acad. Sci.* **110**, 4309–4314 (2013).
62. Li, X. et al. Changes in precipitation extremes in the Yangtze River Basin during 1960–2019 and the association with global warming, ENSO, and local effects. *Sci. Total Environ.* **760**, 144244 (2021).
63. Guo, R., Zhu, Y. & Liu, Y. A comparison study of precipitation in the poyang and the dongting lake basins from 1960–2015. *Sci. Rep.* **10**, 3381 (2020).
64. Rodell, M. et al. Emerging trends in global freshwater availability. *Nature* **557**, 651–659 (2018).
65. Huang, Y. et al. Estimation of human-induced changes in terrestrial water storage through integration of GRACE satellite detection and hydrological modeling: A case study of the Yangtze River basin. *Water Resour. Res.* **51**, 8494–8516 (2015).
66. Shamsudduha, M., Taylor, R. G. & Longuevergne, L. Monitoring groundwater storage changes in the highly seasonal humid tropics: Validation of GRACE measurements in the Bengal Basin. *Water Resour. Res.* **48** (2012).
67. Jing, W. et al. Variations in terrestrial water storage in the Lancang-Mekong river basin from GRACE solutions and land surface model. *J. Hydrol.* **580**, 124258 (2020).
68. Seneviratne, S. I. et al. Investigating soil moisture–climate interactions in a changing climate: A review. *Earth-Sci. Rev.* **99**, 125–161 (2010).
69. Lutz, A. F., Immerzeel, W. W., Shrestha, A. B. & Bierkens, M. F. P. Consistent increase in High Asia's runoff due to increasing glacier melt and precipitation. *Nat. Clim. Change* **4**, 587–592 (2014).
70. Nepal, S. & Shrestha, A. B. Impact of climate change on the hydrological regime of the Indus, Ganges and Brahmaputra river basins: a review of the literature. *Int. J. Water Resour. Dev.* **31**, 201–218 (2015).
71. Mittal, N., Mishra, A., Singh, R. & Kumar, P. Assessing future changes in seasonal climatic extremes in the Ganges river basin using an ensemble of regional climate models. *Clim. Change* **123**, 273–286 (2014).
72. Chandel, V. S. & Ghosh, S. Components of himalayan river flows in a changing climate. *Water Resour. Res.* **57**, e2020WR027589 (2021).
73. Cortés, J. et al. Where are global vegetation greening and browning trends significant? *Geophys. Res. Lett.* **48**, e2020GL091496 (2021).
74. Yoon, Y. et al. Evaluating the uncertainty of terrestrial water budget components over high mountain Asia. *Front. Earth Sci.* **7** (2019).
75. Müller Schmied, H. et al. Variations of global and continental water balance components as impacted by climate forcing uncertainty and human water use. *Hydrol. Earth Syst. Sci.* **20**, 2877–2898 (2016).

76. Song, C., Huang, B., Ke, L. & Ye, Q. Precipitation variability in High Mountain Asia from multiple datasets and implication for water balance analysis in large lake basins. *Glob. Planet. Change* **145**, 20–29 (2016).

77. Ma, L. et al. Evaluation of precipitation from the ERA-40, NCEP-1, and NCEP-2 Reanalyses and CMAP-1, CMAP-2, and GPCP-2 with ground-based measurements in China. *J. Geophys. Res. Atmospheres* **114**, D09105 (2009).

78. You, Q., Min, J., Zhang, W., Pepin, N. & Kang, S. Comparison of multiple datasets with gridded precipitation observations over the Tibetan Plateau. *Clim. Dyn.* **45**, 791–806 (2015).

79. Zhang, J., Yao, F., Zheng, L. & Yang, L. Evaluation of grassland dynamics in the northern-tibet plateau of china using remote sensing and climate data. *Sensors* **7**, 33123328 (2007).

80. Andermann, C., Bonnet, S. & Gloaguen, R. Evaluation of precipitation data sets along the Himalayan front. *Geochem. Geophys. Geosystems* **12**, Q07023 (2011).

81. Funk, C. et al. The climate hazards infrared precipitation with stations—a new environmental record for monitoring extremes. *Sci. Data* **2**, 150066 (2015).

82. Yatagai, A. et al. APHRODITE: constructing a long-term daily gridded precipitation dataset for Asia based on a dense network of rain gauges. *Bull. Am. Meteorol. Soc* **93**, 1401–1415 (2012).

83. Maussion, F. et al. Precipitation seasonality and variability over the Tibetan Plateau as resolved by the high Asia reanalysis. *J. Clim* **27**, 1910–1927 (2014).

84. Sheffield, J., Goteti, G. & Wood, E. F. Development of a 50-year high-resolution global dataset of meteorological forcings for land surface modeling. *J. Clim* **19**, 3088–3111 (2006).

85. Tapley, B. D., Bettadpur, S., Ries, J. C., Thompson, P. F. & Watkins, M. M. GRACE measurements of mass variability in the Earth system. *Science* **305**, 503–505 (2004).

86. Save, H., Bettadpur, S. & Tapley, B. D. High-resolution CSR GRACE RL05 mascons. *J. Geophys. Res. Solid Earth* **121**, 7547–7569 (2016).

87. Wahr, J., Molenaar, M. & Bryan, F. Time variability of the Earth's gravity field: Hydrological and oceanic effects and their possible detection using GRACE. *J. Geophys. Res. Solid Earth* **103**, 30205–30229 (1998).

88. Tapley, B. D. et al. Contributions of GRACE to understanding climate change. *Nat. Clim. Change* **9**, 358–369 (2019).

89. Loomis, B. D. et al. Water storage trends in high mountain Asia. *Front. Earth Sci.* **7**, 235 (2019).

90. Deng, H., Pepin, N. C., Liu, Q. & Chen, Y. Understanding the spatial differences in terrestrial water storage variations in the Tibetan Plateau from 2002 to 2016. *Clim. Change* **151**, 379–393 (2018).

91. Meng, F., Su, F., Li, Y. & Tong, K. Changes in terrestrial water storage during 2003–2014 and possible causes in Tibetan Plateau. *J. Geophys. Res. Atmospheres* **124**, 2909–2931 (2019).

92. Mann, H. B. Nonparametric tests against trend. *Econometrica* **13**, 245–259 (1945).

93. Kendall, M. G. *Rank correlation methods.* (Griffin, 1948).

94. Yue, S., Pilon, P. & Cavadias, G. Power of the Mann–Kendall and Spearman's rho tests for detecting monotonic trends in hydrological series. *J. Hydrol.* **259**, 254–271 (2002).

95. Su, C.-H. et al. Homogeneity of a global multisatellite soil moisture climate data record. *Geophys. Res. Lett.* **43**, 245–11,252 (2016).

96. Albergel, C. et al. Skill and global trend analysis of soil moisture from reanalyses and microwave remote sensing. *J. Hydrometeorol* **14**, 1259–1277 (2013).

97. Timme, N., Alford, W., Flecker, B. & Beggs, J. M. Synergy, redundancy, and multivariate information measures: an experimentalist's perspective. *J. Comput. Neurosci.* **36**, 119–140 (2014).

98. Williams, P. L. & Beer, R. D. Nonnegative decomposition of multivariate information. *ArXiv10042515 Math-Ph Physicsphysics Q-Bio* (2010).

99. Friedl, Mark & Sulla-Menashe, Damien MCD12Q1 MODIS/Terra+Aqua Land Cover Type Yearly L3 Global 500m SIN Grid V006. https://doi.org/10.5067/MODIS/MCD12Q1.006 (2019).

Author contributions

F.Z.M and S.V.K. contributed with conceptualization, data analysis, and writing. C.A. and S.P.M. contributed with the data acquisition. S.V.K. was responsible for funding acquisition. All authors have read and agreed to the published version of the manuscript.

Competing interests

The authors declare no competing interests.

Additional information

Supplementary information The online version contains supplementary material available at https://doi.org/10.1038/s43247-022-00374-0.

Correspondence and requests for materials should be addressed to Fadji Zaouna Maina.

Peer review information *Communications Earth & Environment* thanks Kumar Mainali and the other, anonymous, reviewer(s) for their contribution to the peer review of this work. Primary Handling Editor: Joe Aslin. Peer reviewer reports are available.

Reprints and permission information is available at http://www.nature.com/reprints

Publisher's note Springer Nature remains neutral with regard to jurisdictional claims in published maps and institutional affiliations.